PCCP



PAPER



Cite this: Phys. Chem. Chem. Phys., 2021, 23, 14678

Structural and energetic properties of OC-BX₃ complexes: unrealized potential for bondstretch isomerism

Jordan A. Munos, Diego T. Lowney and James A. Phillips **D**

We have explored the structural and energetic properties of $OC-BX_3$ (X = F, Cl, or Br) complexes using computations and low-temperature infrared spectroscopy. Quantum-chemical calculations have provided equilibrium structures, binding energies, vibrational frequencies, and B-C potential energy curves. The $OC-BF_3$ system is a weak, long-bonded complex with a single minimum on the B-C potential (R(B-C) = 2.865 Å). For the remaining two complexes, OC-BCl₃ and OC-BBr₃, computations predict two stable minima on their B-C potential curves. The BCl_{τ} system is a weak complex with a long bond (R(B-C) = 3.358 Å), but it exhibits a secondary, meta-stable minimum with a short bond length of 1.659 Å. For OC-BBr3, the system is a weak complex with a relatively short bond of 1.604 Å (according to wB97X-D/aug-cc-pVTZ), but also has a secondary minimum at R(B-C) = 3.483 Å. This long-bond structure is the global minimum according to CCSD/ aug-cc-pVTZ. In addition, the long-bond forms of both OC-BCl₃ and OC-BBr₃ were observed in matrixisolation IR experiments. The measured CO stretching frequencies were 2145 cm⁻¹ and 2143 cm⁻¹, respectively. No signals due to the short-bond forms of OC-BCl₃ and OC-BBr₃ were observed.

Received 20th May 2021, Accepted 27th June 2021

DOI: 10.1039/d1cp02230i

rsc.li/pccp

Introduction

Interest in molecular complexes and their structural and energetic properties has continued for years since the 1960's. 1,2 One reason for this continued interest stems from on-going computational chemistry research. From a practical standpoint, developers of various density functional theory (DFT) methods such as M06 and M06-2X^{3,4} have used the "Charge Transfer Database" (in part) to validate energy results. Computational investigations have also provided a great deal of insight into the complex and often ambiguous the bonding interactions in these systems, which has been illustrated in a few comprehensive, comparative studies.^{5,6} These efforts identified a continuous range of interactions that spans from van der Waals interactions to covalent bonds, and moreover, they found that no one feature (e.g., electrostatics, charge-transfer, etc.) contributed a fixed amount the binding energy, or paralleled strength in any consistent, systematic manner. In addition, computations have led to a more systematic classification that makes reference to the geometries about the electron deficient regions of the acceptor center. These are known as " σ -hole" and " π -hole" interactions. ^{7–9} Common examples of σ -hole interactions include hydrogen bonding, 7,8 halogen bonding, 7,8 and MX₄

Department of Chemistry and Biochemistry, University of Wisconsin - Eau Claire, 105 Garfield Ave., Eau Claire, WI 45702, USA. E-mail: phillija@uwec.edu; Tel: +1-715-836-5399

coordinate bonds. The most common examples of π -holes are in Group 13 (MX₃) acceptors such as BCl₃.¹⁰

Another reason for the on-going interest in these systems is that some molecular complexes undergo major changes in structure when going from the gas phase to the solid state or other stabilizing, condensed-phase environment. Perhaps the most vivid examples are the nitrile–BF₃ complexes^{11,12} – π -hole complexes - for which there are documented structural changes across a range of environments. The specific signature of this effect is a contraction of the B-N distance and a distortion of the acceptor molecule (BF₃), and the clearest illustrations are gas-solid structure differences. For example, the gas-phase structure of CH3CN-BF3 has a B-N distance of 2.011 Å, 13 but the donor-acceptor bond contracts by 0.381 Å in the solid state, to a distance of 1.630 Å. 12,14 In the case of HCN-BF₃, ¹⁵ FCH₂CN-BF₃, ¹⁶ and ClCH₂CN-BF₃, ¹⁶ the effect is even more extreme with B-N distances contracting by 0.7 Å to 0.8 Å between the gas phase and the solid state.

For the nitrile-BF₃ systems, significant changes in structure can even be induced by inert media such as noble gas matrices, and this sensitivity stems from an extreme anharmonicity in the donor-acceptor potential. 11 The experimental signature of this effect is a shift in a key acceptor mode in the infrared (IR) spectra of the complexes (relative to the free acceptor), which has been shown to parallel the B-N distance, and thus reflects a progressive contraction of the B-N bond. 17 Scans of the donoracceptor potential have identified a distinct shape in these

medium-sensitive systems, characterized by a long equilibrium distance and a gentle rise toward the inner wall of the curve. 18,19 The generalized mechanism for condensed-phase structural change is as follows; in dielectric media, the inner region is preferentially stabilized, such that the minimum shifts inwards via solvent interactions. Models based on this effect reproduce the observed, ~ 0.7 Å contraction in the B-N bond for FCH₂CN-BF₃. ¹⁸ In an extreme case, similar models predict a 1.0 Å shortening for CH₃CN-SiF₄, ¹⁹ from 3.0 Å in the gas phase to 2.0 Å in a dielectric media of with $\varepsilon = 20$.

In subsequent studies of the BCl3 analogs of these nitrile-BF₃ systems, ^{20,21} a different, novel aspect of the intermolecular potential was discovered - the occurrence of two distinct minima along the B-N coordinate. These minima, corresponding to so called "short-" and "long-bond" structures, is reminiscent of a phenomenon known as "bond-stretch isomerism," which has been a contentious topic since the 1990's. 22,23 To some extent, the idea of bond-stretch isomers had been dismissed due to the lack of experimental evidence, yet theoretical predictions of such systems continue to arise.24-26 Nonetheless, computational results for CH₃CN-BCl₃ predicted two distinct minima at 1.601 Å and 2.687 Å²⁰ separated by a significant barrier, which persisted at high-levels of theory (CCSD/aug-cc-pVTZ). However, only signals due to the short-bond form were observed in matrixisolation IR experiments, in part because overlapping signals in the nitrile stretching region impeded assignment of peaks due to the long-bond structure.

Similar results were obtained when this work was extended to FCH₂CN-BCl₃ and ClCH₂CN-BCl₃.²¹ In the case of CH₃CN-BCl₃, the short-bond form was much lower in energy, but for FCH₂CN-BCl₃ and ClCH₂CN-BCl₃, ²¹ the addition of halogens weakened the bond, rendering the two minima much closer in energy. The binding energies (global minima) for the short-bond forms were 5.3 kcal mol⁻¹ and 6.3 kcal mol⁻¹ for FCH₂CN-BCl₃ and ClCH₂CN-BCl₃, respectively. Notably, the energy of the longbond forms (3.2 kcal mol⁻¹ and 3.3 kcal mol⁻¹) were much less affected by halogen substitution, and were nearly equal to the for CH₃CN-BCl₃. However, in spite of the fact that halogen substitution did equalize the energies of the two minima to some extent, only signals for the short-bond form were observed in matrix-IR experiments.

Here, we extend this work to similar systems for which there are some other advantageous features. Carbon monoxide (CO) is isovalent with nitriles, but is a much simpler donor with only one vibrational frequency in a sparse region of the spectrum, which would minimize overlap with other signals, and presumably facilitate the observation of distinct, but often slight, frequency shifts. In addition, we explore a wider range of halogens on the BX₃ acceptors. This manuscript will report the structural and energetic properties of OC-BX₃ (X = F, Cl or Br) complexes, including equilibrium structures, predicted gas-phase frequencies, and potential energy curves, via quantum-chemical computations and IR experiments in Ar and Ne matrices. The BCl₃ and BBr₃ complexes with CO both show potential for the observation of distinct structures with different B-C minima, particularly in the latter case. By contrast, OC-BF3 is a weakly-bonded system with a

known experimental structure, 27 which did provide a valuable computational benchmark.

Materials and methodology

Computations

Post Hartree-Fock and DFT calculations were performed using Gaussian09 B.01²⁸ and Gaussian16 C.01.²⁹ Symmetry was constrained to C_{3v} geometry throughout these computational studies. Optimizations were performed with convergence criteria set using the "opt = tight" option, and an ultrafine grid was employed for all DFT and MP2 calculations.

Overall, we utilized multiple DFT methods (M05,30 M06,3 M06-2X,³ ωB97X-D,³¹ M08-HX,³² M11,³³ MN12-SX,³⁴ and MN15³⁴) along with MP235 and CCSD35 with the aug-cc-pVTZ basis set.35 A validation study was conducted, as in previous work by the group, which was based on acceptor frequencies and experimental gasphase structures. 16,20 The structures and binding energies reported here are from ωB97X-D, which had the smallest RMS error when predicting experimental BF3 and BCl3 frequencies $(7.23 \text{ cm}^{-1} \text{ and } 8.75 \text{ cm}^{-1} \text{ for BF}_3 \text{ and BCl}_3, \text{ respectively}).^{36} \text{ In}$ addition, ωB97X-D also most accurately predicted the experimental structure of OC-BF₃ (0.023 Å difference in the B-C distance).²⁷ However, we do note that M06 was somewhat more accurate in predicting BBr₃ frequencies (RMS_{M06} = 3.2 cm^{-1} and RMS_{ω B97X-D} = 13.5 cm⁻¹). We note here that none of these methods explored were particularly effective in predicting the frequency of free CO (within 30 cm^{-1}). In the end we observed only peaks in the CO region, and thus utilized predicted shifts (as opposed to absolute frequency values) to assist in our peak assignments.

The B-C potential was mapped in a pointwise manner from 1.4 Å to 3.0 Å in steps of 0.1 Å using the following methods: M05, M06, M06-2X, ωB97X-D, MP2, and CCSD, all with the aug-cc-pVTZ basis set. The energies on the CCSD curves were based on MP2 geometries. Among these methods, ωB97X-D most closely matched the CCSD energies along these curves, but most methods—aside from MP2—were qualitatively similar. The notable exception is that the CCSD energies identify a different global minimum in the case of OC-BBr₃ (see below), but the overall energy difference is slight.

Materials

CO (99.0%) was obtained from Sigma-Aldrich and used without further purification. BCl₃ (99.9%) was obtained from Sigma-Aldrich and was transferred to a sample tube by filling a 2 L bulb to a pressure of 1-2 atm, and then condensed in a 50 mL sample tube with liquid nitrogen. Both BCl₃ and BBr₃ are highly corrosive substances which readily react with trace amounts of water to produce HCl and HBr, respectively. Further purification of the BCl₃ sample was necessary to remove a persistent HCl impurity, and was achieved through a two-step process: first freeze-pump-thaw cycles at the temperature of liquid nitrogen (77 K), then the sample was subjected to active vacuum in several 10-30 second intervals at 183 K via a liquid nitrogen/methanol bath. BBr3 was obtained at a purity of 99.995% from Sigma-

Aldrich, and was transferred to a sample tube via a disposable pipet, and prior to use was further purified by freeze–pumpthaw cycles in a liquid nitrogen bath at 77 K. Ar (99.999%) and Ne (99.999%) were obtained from Praxair and used with no further purification.

Matrix-isolation IR spectra

IR spectra were collected using two previously described matrixisolation apparatuses. Initial spectra in argon matrices were collected using a ~10 K system. 37,38 that utilizes a Cryomech ST15 optical cryostat and a Nicolet Avatar iS20 FTIR spectrometer at 1.0 cm⁻¹, averaging 400 scans per spectrum. Matrix samples were deposited on a KBr window, and the temperature was maintained using a Scientific Instruments 9600-1 temperature controller with a single Si diode located at the end of the second refrigeration stage. The majority of experiments were conducted in neon matrices on a 4 K system^{20,39} that employs a Janis SHI-4-5 optical cryostat and a Thermo Nexus 670 FTIR. The resolution was 1.0 cm⁻¹, and 400 scans were averaged for each spectrum. Matrix samples were deposited onto a gold mirror and spectra were collected by reflecting the IR beam off the sample mirror ($\sim 45^{\circ}$) and onto an external (DTGS) detector. Samples were prepared in 2 L glass bulbs on a glass manifold (Chemglass) evacuated with a diffusion pump (Chemglass) by making separate gas mixtures containing either CO or BX₃ (X = Cl or Br) in Ar or Ne. For experiments, matrix samples were deposited by simultaneous flow of gas mixtures in separate lines that merge immediately before the mirror. A final set of experiments using single mixtures containing both guest gases in the same bulb and deposition line yielded identical spectra. Mixtures were deposited at temperatures ranging from 3.5 K to 6 K and in most experiments we ran two to four 60 minute depositions, after which most samples were annealed at temperatures of 8-9 K for 30 minutes to one hour with spectra recorded after each deposition and anneal. Flow rates typically ranged from 1 to 10 mmol h⁻¹ with mixture concentrations ranging from 1/32-1/2%. It should be noted that faster deposition rates seemed to reduce the amount of HX in the spectra, relative to BX₃. This suggests decomposition in the deposition plumbing, in spite of the fact that the lines were mainly Teflon, with as little metal plumbing as possible in an effort to minimize this outcome.²⁰

Bulk reactivity

To ensure that we could perform the single-bulb experiments described above, we examined the direct reaction of CO and BCl₃ or BBr₃. In this experiment, $\sim\!50$ torr each of BBr₃ and CO were introduced into a 100 mL reaction flask on our preparatory manifold. The gases were allowed to mix for $\sim\!20$ minutes before sitting in an ice bath for $\sim\!10$ minutes. Neither measure produced a visible reaction product.

Results and discussion

Equilibrium structures

Due to previous work on $\mathrm{CH_3CN-BCl_3}^{20}$ and $\mathrm{XCH_2CN-BCl_3}^{21}$ we expected two distinct structures with different B–C distances

for OC–BCl₃ and OC–BBr₃. Thus, when searching for equilibrium structures we started the optimizations from two different geometries with short (1.6 Å) and long (3.0 Å) B–C distances. As noted above, we used a variety of DFT methods as well as MP2 and CCSD, settling on ω B97X-D for most of the structure and binding energy results reported in this manuscript. All other methods produced relatively consistent results.

All structural parameters for OC-BF3 are shown in Fig. 1. This complex is a weakly-bonded system and has a single, distinct structure with a long B-C distance (2.865 Å) and a binding energy of 2.5 kcal mol⁻¹. These results are consistent with the recently-updated structure of OC-BF₃, ²⁷ which puts the B-C distance at 2.888 Å. For context, the van der Waals radii⁴⁰ for carbon (1.7 Å) and boron (1.8 Å) add to a sum of 3.5 Å, 0.6 Å longer than the B-C distance of OC-BF₃, while the sum of the covalent radii⁴¹ for carbon (0.77 Å) and boron (0.84 Å) is 1.61 Å, significantly shorter than the calculated B-C distance of 2.865 Å. The acceptor molecule (BF₃) has little distortion from its trigonal-planar geometry; the F-B-C angle is 91.3°. Compared to HCN-BF₃, a similar, isoelectronic complex,^{5,42} OC-BF₃ has a considerably longer donor-acceptor distance. For HCN-BF₃, the experimental B-N distance is 2.473 Å, 5,42 almost an angstrom shorter than the van der Waals radii. The binding energy of the HCN complex is 5.0 kcal mol⁻¹ via ωB97X-D/aug-cc-pVTZ (present work), which makes the complex twice as strong as the analogous CO complex, which has a binding energy of $2.5 \text{ kcal mol}^{-1}$.

By contrast, we predict two structures for the OC–BCl $_3$ and OC–BBr $_3$ complexes, which we refer to as the "short-" and "long-bond" forms henceforth. The long-bond forms of OC–BCl $_3$ and OC–BBr $_3$ are generally similar to the OC–BF $_3$ complex; all are weakly-bonded structures with little distortion in the acceptor subunit. Both have slightly longer B–C distances than the BF $_3$ complex, 3.358 Å and 3.485 Å, respectively, much closer to the sum of the carbon and boron van der Waals radii. Both complexes exhibit similar X–B–X and X–B–C angles with the former being 120°, and the latter being 90.5° and 90.4° respectively, indicating slightly less distortion than in OC–BF $_3$. A complete set of structural parameters are included in Fig. 2 and 3. Binding energies for the Cl- and Br-containing complexes are both 1.5 kcal mol $^{-1}$, which are 1.0 kcal mol $^{-1}$ smaller in magnitude than the analogous BF $_3$ complex.

These long-bond structures resemble their analogs in the nitrile-BCl₃ systems (e.g., CH₃CN-BCl₃).²⁰ Again, while the

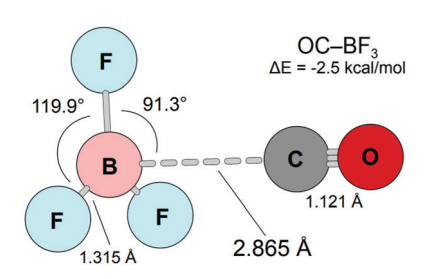


Fig. 1 Structure and binding energy for OC-BF $_3$ via ω B97X-D/aug-cc-pVTZ.

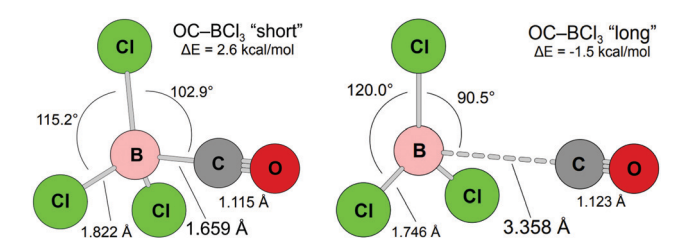


Fig. 2 Structures and binding energies for two equilibrium structures of OC-BCl₃ via ωB97X-D/aug-cc-pVTZ.

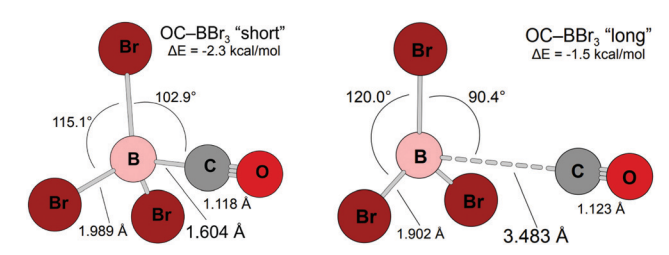


Fig. 3 Structures and binding energies for two equilibrium structures of OC-BBr₃ via ωB97X-D/aug-cc-pVTZ.

donor-acceptor distances cannot be directly compared due to differences in the atoms of the interaction, an indirect comparison can be based on van der Waals radii. For CH₃CN-BCl₃, the predicted MP2/aug-cc-pVTZ B-N distance is 2.687 Å, 0.663 Å shorter than the sum of the van der Waals radii, while the B-C distances for the OC-BCl3 and OC-BBr3 forms differ by only 0.142 Å and 0.015 Å respectively. This points to a slightly weaker interaction in the long-bond forms of the OC-BX3 complexes, compared to CH3CN-BCl3. This observation is substantiated by the values of the binding energies; which are 1.5 kcal mol⁻¹ for both complexes. By contrast, $CH_3CN-BCl_3$ ($\Delta E = -4.9$) is more strongly bound than the CO complexes by almost 3.5 kcal mol⁻¹. Overall, both longbond forms of OC-BCl₃ and OC-BBr₃ are fairly weak complexes, with little distortion in the acceptor molecule, and long donoracceptor distances approaching the sum of their respective van der Waals interaction radii.

Turning now to the short-bond structures for both the Cl- and Br-complexes, we found both systems exhibit large distortions of the acceptor molecule due to the short B-C distances. For $OC-BCl_3$, the B-C distance is 1.659 Å, which is 0.055 Å longer than OC-BBr₃ (R(B-C) = 1.604 Å). The X-B-C angles are both 102.9°. In these structures, both B-C distances are close to the sum of the covalent radii of boron (0.84 Å) and carbon (0.77 Å) which is 1.61 Å, an indication that the interactions in these short-bond forms involve some degree of charge transfer and/or covalent bonding. In contrast to their long-bond counterparts, the binding energies of these structures, are not similar. For OC-BCl₃, the energy lies above that of the separated fragments $(\Delta E = +2.5 \text{ kcal mol}^{-1})$, while for OC-BBr₃ the overall energy lies 0.8 kcal mol^{-1} below its long-bond counterpart ($\Delta E =$ -2.3 kcal mol⁻¹). However, we note that the CCSD/aug-ccpVTZ energies, as inferred from the B-C potential scans

(see below), indicate that the long-bond form is actually the global energy minimum. As a whole, the situation with these systems resembles that for the N₂-BH₃ complex, 43 in which the B-N distance is quite short, but the binding energy is small; the bonding interactions are offset by significant repulsive interactions between donor and acceptor.

Structurally, these short-bond forms resemble the analogous short-bond structure for the CH₃CN-BCl₃ system.²⁰ The B-N distance is 1.601 Å, a bit longer than the sum of the covalent radii, by 0.051 Å. The OC-BCl₃ complex has a donor-acceptor distance that is also just longer than the sum of the covalent radii (0.049 Å), while for OC-BBr₃ the value is 0.006 Å shorter than that predicted by covalent radii. The distortion of the Cl-B-N angle in the short-bond CH₃CN-BCl₃ is almost 2° larger than the analogous angle in the OC-BX₃ complexes, and the binding energy of the nitrile complex is larger. These indicate a stronger interaction for CH₃CN-BCl₃, relative to the short-bond OC-BX₃ structures, but they are qualitatively similar nonetheless.

For a more classic example, we turn to H₃N-BCl₃.^{5,44} Here the B-N distance is 1.618 Å, again just longer (0.068 Å) than the sum of the covalent radii. However, the binding energy for the ammonia complex is significantly larger in magnitude than those of the CO complexes; 28.2 kcal mol⁻¹ (via MP2/ 6-31+G(2d,p)/MP2/6-31+G(2d,p). Compared to the shortbond form of CH₃CN-BCl₃, the ammonia complex has a longer bond, but stronger interaction. An analogous trend had been noted previously in RCN-BH3 complexes, 45 which have shorter B-N bonds and a smaller $|\Delta E|$ compared their amine counterparts. The difference is that ammonia has an sp³-like lone pair, which is more extended in space than the sp-like lone pair of the nitriles, allowing for overlap to occur at a longer distance. By contrast, the sp-like lone pair of the CH₃CN extends to a lesser degree, and must be closer to the acceptor molecule for significant overlap to occur. At these short distances, the π electrons of the C-N triple bond and the halogens of the acceptor molecule repel each other significantly, which (as noted above for N2-BH3) raises the overall energy, offsetting the energetically-favorable bonding interactions. The end result is an interaction that is shorter and weaker for the CH3CN complex than for NH₃-BH₃. In the present case, OC-BCl₃ and OC-BBr₃ are structurally indicative of significant covalent or charge-transfer interactions, with short donor-acceptor distances close to the sum of their covalent radii and large distortions of the acceptor molecules. However, from an energetic standpoint these complexes are fairly weak, and by analogy to the nitrile-BX3 systems, 11 we presume this also stems from the repulsive contribution to the energy at these inner distances.

Donor-acceptor potentials

Fig. 4 through 6 display the boron-carbon potential energy curves computed via a variety of DFT methods along with MP2 and CCSD and the aug-cc-pVTZ basis set. These curves offer two major observations; one being the relative energy between the two minima of the Cl- and Br-containing complexes, the other being the barrier that exists between these two distinct minimum-energy structures. For OC-BF3, we note that the

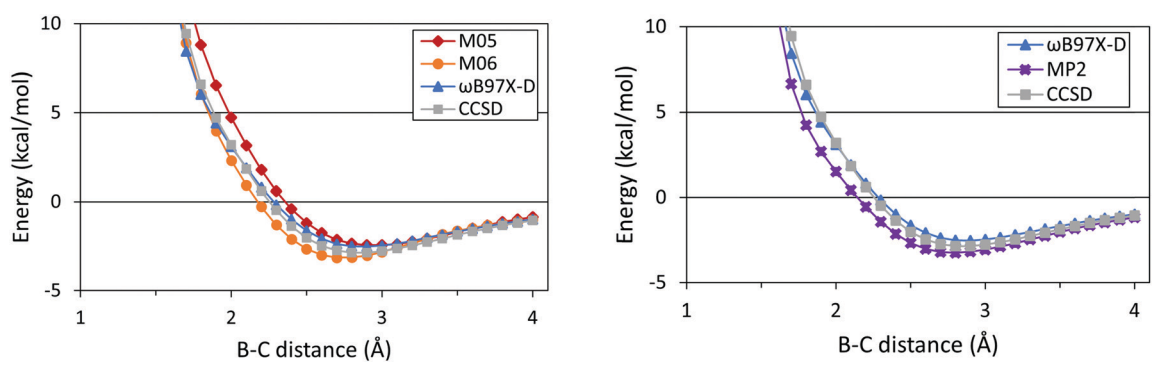


Fig. 4 Calculated B-C bond potentials for OC-BF3 using hybrid DFT methods (and CCSD) with the aug-cc-pVTZ basis set (left) and post-HF methods and ωB97X-D with the aug-cc-pVTZ basis set (right). An M06-2X/aug-cc-pVTZ curve was calculated but was not included because it was essentially superimposed on the M06 curve.

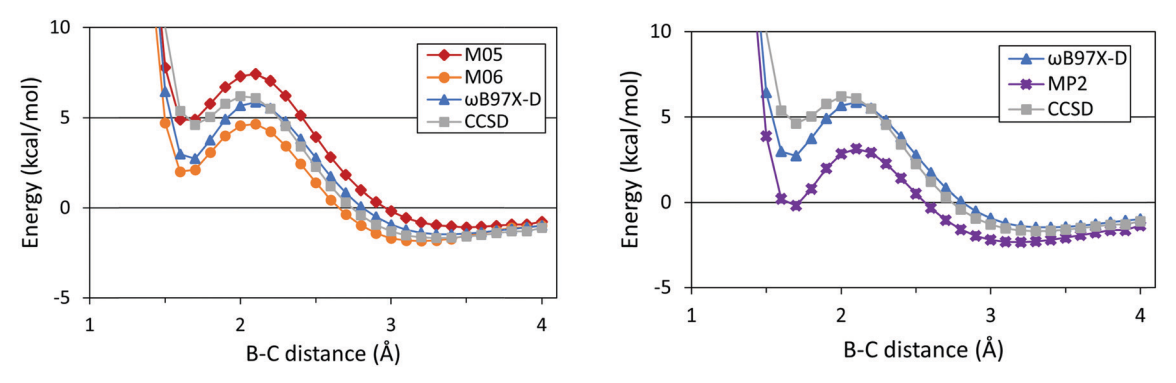


Fig. 5 Calculated B-C bond potentials for OC-BCl₃ using hybrid DFT methods (and CCSD) with the aug-cc-pVTZ basis set (left) and post-HF methods and ωB97X-D with the aug-cc-pVTZ basis set (right). An M06-2X/aug-cc-pVTZ curve was calculated but was not included because it was essentially superimposed on the M06 curve.

curve resembles those of systems prone to condensed phase media effects, with its relatively long minimum and gentle rise towards the inner portion of the curve. 11 Interestingly, the system has been studied via matrix-IR, 46,47 and the measured frequencies nearly agree with our predictions, but there is the slightest indication of a matrix-induced contraction of the B-C bond. The B-F asymmetric stretching bands of OC-BF₃ had

been previously observed at 1438.7/1437.3 cm⁻¹ and 1441 cm⁻¹ in argon matrices. 46,47 In this work, we predict a frequency at $1444~\text{cm}^{-1}$ ($\omega B97X\text{-D/aug-cc-pVTZ}$) for this band. This is in reasonable agreement, however, the 3-7 cm⁻¹ red shift between the matrix data and the gas-phase predictions is consistent with a slight compression of the B-C bond (though the difference is arguably near the RMS error in our frequency predictions).

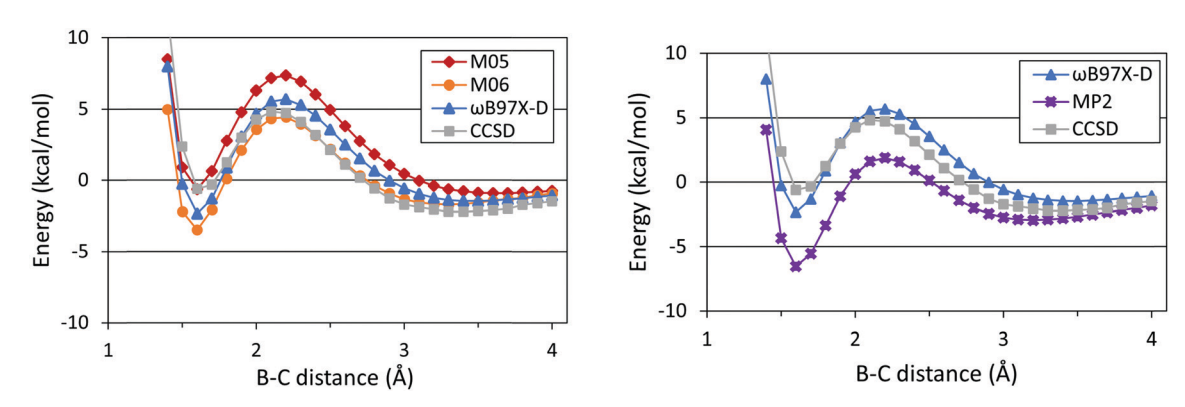


Fig. 6 Calculated B-C bond potentials for OC-BBr₃ using hybrid DFT methods (and CCSD) with the aug-cc-pVTZ basis set (left) and post-HF methods and ωB97X-D with the aug-cc-pVTZ basis set (right). An M06-2X/aug-cc-pVTZ curve was calculated but was not included because it is essentially superimposed on the M06 curve.

For OC-BCl₃, the energy maximum occurs around 2.1 Å $(+5.9 \text{ kcal mol}^{-1})$ with the energy $+7.4 \text{ kcal mol}^{-1}$ relative to the outer minimum, and the two minima are 4.1 kcal mol⁻¹ apart. For OC-BBr₃, the barrier occurs at 2.2 Å (+5.7 kcal mol⁻¹) with the energy +7.2 kcal mol⁻¹ relative to the outer minimum. The two minima are closer in energy to each other than those of the BCl₃ complex with a difference of only 0.8 kcal mol⁻¹ between them. It should be noted that CCSD predicts a significantly higher energy along the inner part of the curve (relative to all DFT methods), and indicates that the long-bond structure is the global energy minimum. Moreover, this result is more consistent with what we observe in our experiments (see below).

Fig. 7 shows two different overlays for the three complexes, one for the ωB97X-D potentials and another for the CCSD potentials, to facilitate comparison between the shapes of the respective curves. The graphs not only display the clear difference in energy between the two minima for the BCl3 and BBr₃ complexes; but also, the difference in the calculated energies between DFT and CCSD. Again, for ωB97X-D, the calculations predict a much lower-energy inner minimum for BBr₃ with a higher-energy outer minimum, while CCSD does the exact opposite. For the BF3 complex, CCSD predicts a similar energy rise to that for ωB97X-D, and the minimum energy points lie at nearly the same B-C distances, 2.9 Å and 2.8 Å for ωB97X-D and CCSD, respectively. Another observation these graphs lend themselves to is an explanation as to why BF₃ does not show a barrier, and in turn, two distinct structures like the BCl₃ and BBr₃ complexes. Overall, this situation mimics what we encountered previously for nitrile-BX₃ complexes, ¹¹ and rationalized via energy decomposition analyses. 45 In the systems with the larger halogens (Cl, and presumably Br), the barrier results from repulsion between the halogens and the π electrons on C-N or C-O, which set in at fairly long distances. At shorter distances, these repulsions are offset by bonding interactions (more or less). This effect has been further illustrated in a study of the HCN-BCl3 complex, by comparing the B-N potentials obtained both with and without relaxed fragment geometries.²⁶ For BF₃ systems, the favorable bonding interactions and π -halogen repulsions set in at similar distances, rendering the potentials flat (and leading to medium effects for nitrile-BF₃ systems).¹¹

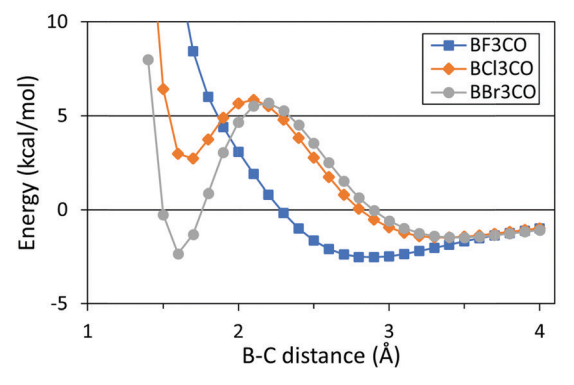
Table 1 Summary of boron charges and LUMO energies

Acceptor molecule	$q_{ m\scriptscriptstyle B}$ (e)	E_{LUMO} (eV)	
BF ₃ BCl ₃	+1.40 +0.34	+0.044 +0.002	
BBr ₃	+0.06	-0.013	

Lastly, the overall trends in the energies in the short- and long-bond regions of the curve can be rationalized in terms of key acceptor properties (i.e., charge on the boron atom and LUMO energies), which are displayed in Table 1. The energy in the short-bond region parallels LUMO energies (BBr₃ < BCl₃ < BF₃), which one might expect to correlate with stronger bonding interactions (BBr₃ > BCl₃ > BF₃). On the other hand, the charge on the central atom is greatest on BF₃, and this seems consistent with OC-BF₃ having the lowest energy minimum in the long bond region (though arguably this effect is convoluted with the barrier stemming from the onset of repulsions for BCl₃ and BBr₃).

IR spectra and frequencies

We recorded IR spectra of OC-BCl3 and OC-BBr3 in lowtemperature matrices, focusing mainly on solid neon, although we did perform some CO/BCl3 experiments in solid argon as well. For both OC-BCl3 and OC-BBr3, we were able to assign one band in the CO region to the 1:1 OC-BX₃ complex, and this guided by predicted frequency shifts (\omegaB97X-D/aug-cc-pVTZ). Fig. 8 and 9 show, respectively, the spectra in the CO regions for both CO/BCl3 and CO/BBr3 experiments in solid neon. In the OC/BCl₃ data, we see two product peaks that do not appear in the CO (or BCl₃) reference spectra. Of these, we assigned the peak at 2144 cm⁻¹ to the long-bond form of the complex, while the peak at 2154 cm⁻¹ is due to OC-HCl arising from the persistent the HCl impurity. As noted above, while specific frequency predictions agree only marginally with what is observed in experiments, calculated shifts (complex - free CO) are reasonably consistent with observations. For the short-bond form of OC-BCl₃, the CO stretching frequency is predicted to be at 2313 cm⁻¹ (shift of +73) and was not observed in the experiments. As for the long-bond form, predictions have a vibration at 2248 cm⁻¹ (+7). A peak at 2145 cm⁻¹ (+4) was



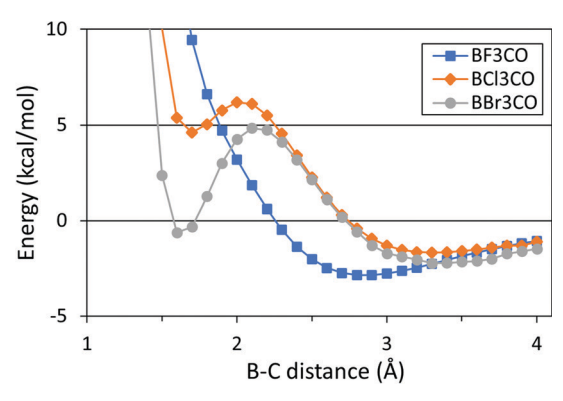


Fig. 7 An overlay of the B-C bond potentials for the series via ωB97X-D/aug-cc-pVTZ (left) and CCSD/aug-cc-pVTZ//MP2/aug-cc-pVTZ (right).

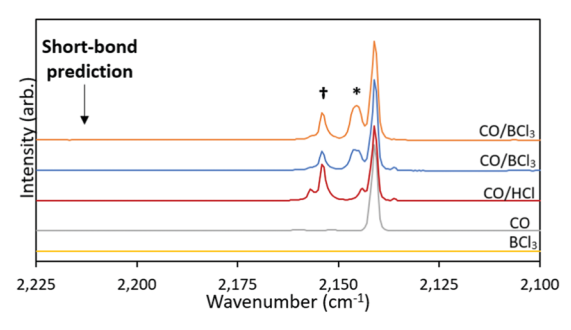


Fig. 8 IR spectrum of OC-BCl₃ in solid Ne. Spectra as marked with the top trace reflecting 30 minutes of annealing at 9 K. The assigned complex peak is marked with an asterisk (*) and the impurity (OC-HCI) peak is marked with a dagger (†). The expected position of the short-bond form of OC-BCl₃ is noted.

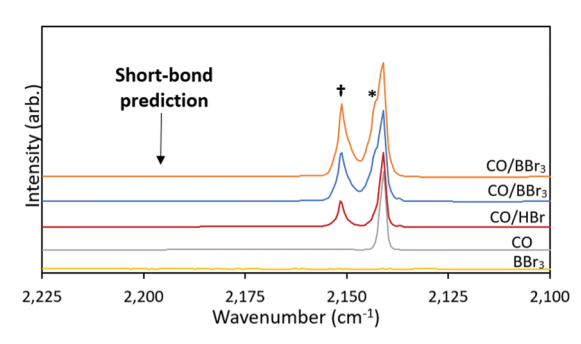


Fig. 9 $\,$ IR spectra of OC-BBr $_3$ in solid Ne. Spectra as marked with the top trace reflecting 30 minutes of annealing at 9 K. The assigned complex peak is marked with an asterisk (*) and the impurity (OC-HBr) peak is marked with a dagger (†). The expected position of the short-bond form of OC-BBr3 is noted.

assigned to the long-bond form. We predict CO stretching frequency of OC-HCl at 2261 cm⁻¹ (+20) and experimentally assigned it to a peak at 2154 cm⁻¹ (+13). Table 2 also includes product band assignments and peak shifts for argon experiments. Peaks were assigned in a similar fashion as described with the neon experiments.

Table 3 shows all peak assignments and shifts for the 1:1 OC-BBr₃ complex. In OC/BBr₃ experiments, we again observed two product peaks at 2143 and 2151 cm⁻¹. The CO stretch for long-bond form was predicted at 2246 cm⁻¹ (+5) and was observed at 2143 cm⁻¹ (+2), as a shoulder on the high-frequency edge of the free CO peak. The CO stretch for the OC-HBr complex

Table 2 Observed and calculated vibrations frequencies of OC-BCl₃

	Frequency (cm ⁻¹)			Shifts (cm ⁻¹)		
	Obs. ^a (Ne)	Obs. ^a (Ar)	Calcd ^b	Obs. ^a (Ne)	Obs. ^a (Ar)	Calcd ^b
OC-BCl ₃ (long) ^c	2145	2143	2248	+4	+6	+7
OC-BCl ₃ (long) ^c OC-BCl ₃ (short) ^d	_	_	2313	_	_	+73
OC-HCl	2154	2153	2261	+13	+16	+20

^a Margin of error: ±1 cm⁻¹. ^b ωB97X-D/aug-cc-pVTZ. ^c Bond length: 3.358 Å. ^d Bond length: 1.659 Å.

Table 3 Observed and calculated vibrational frequencies of OC-BBr₃

	Frequency (cm ⁻¹)		Shifts (cm ⁻¹)
	Obs. ^a (Ne)	Calcd ^b	Obs. ^a (Ne)	Calcd ^b
OC-BBr ₃ (long) ^b	2143	2246	+2	+5
OC-BBr ₃ (short) ^c	_	2230	_	+56
OC-HBr	2151	2244	+10	+3

^a Margin of error: 1 cm⁻¹. ^b ωB97X-D/aug-cc-pVTZ. ^c Bond length: 3.483 Å. ^d Bond length: 1.604 Å.

predicted at 2244 cm⁻¹ (+3), and thus, we assign the peak at 2151 cm⁻¹ (+10) to OC-HBr. The CO stretch of the short-bond form of OC-BBr₃ complex, calculated at 2230 cm⁻¹ (+56), was not observed.

In general, the present result in which we have observed only the long-bond forms is in contrast to our previous work on nitrile-BCl₃ systems, in which only the short-bond forms were observed. In those cases, signals for the long-bond forms may have been obscured due to spectral congestion and CO2 impurity signals. 20,21 In the present case, we were able to observe the very slight shifts induced by the weak interactions in the long-bond forms of OC-BCl₃ and OC-BBr₃, due to the absence of congestion in the CO region. Normally, one would verify matrix-IR peak assignments via the observation of consistent relative intensities across a range of conditions for a given spectral carrier. That is not possible with the observation of a single peak. For these systems, one might expect to observe fairly strong peaks for the 1:1 complexes in the BX₃ asymmetric stretching region, but with BCl3 and BBr3, the occurrence of multiple isotopomers leads to a significant broadening of the free BX₃ signals. This, together with small shifts for the longbond forms, renders these peaks unobservable. Also, the absence of signals due to the short-bond forms in this region, which would be far-shifted from the free BX₃ signals, is further evidence that these structures are not present to any great extent in our matrix samples.

Conclusion

We have conducted a computational and experimental study of the structural and energetic properties of series of OC-BX₃ complexes. The OC-BF3 complex has a singular structure with a long, weak B-C bond, and a potential curve reminiscent of systems prone to slight condensed-phase medium effects. In addition, comparisons between previous experimental data and our predicted frequencies are consistent with a slight compression of the B-C bond in an argon matrix environment. Theoretically, OC-BCl₃ is predicted to have two minimum energy structures, so called "short-" and "long-bond" forms, with B-C distances of 1.659 Å and 3.358 Å, respectively; the latter being the global minimum. However, in matrix-IR experiments we were only able to assign peaks to the longbond form. Much like the BCl₃ complex, OC-BBr₃ also shows the potential for two distinct structures theoretically, with B-C distances of 1.604 Å and 3.408 Å, but the short-bond form is lower in energy according to most methods (CCSD/aug-cc-pVTZ

being the notable exception). But again, matrix-IR spectra show evidence for the long-bond form only. Overall, the trends in the features of the B-C potential energy curves can be rationalized by properties of the BX₃ acceptors, and seem to stem from and illustrate a delicate interplay between attractive and repulsive forces along the B-C coordinate.

Author contributions

Munos: investigation, data curation, formal analysis, writing original draft; Lowney: investigation; Phillips: conceptualization, funding acquisition, methodology, project administration, supervision, writing - review and editing.

Conflicts of interest

There are no conflicts to declare.

Acknowledgements

This work was supported by the National Science Foundation (US) Awards CHE-1566035 and CHE-1626238, as well as the Office of Research and Sponsored Programs at UWEC. This work was made possible via CPU time allotted through the Blugold Supercomputing Cluster (BGSC) at UW-Eau Claire, and via the MERCURY Consortium (supported by National Science Foundation (US) grant #CHE-2018427). Also, J. A. M. and D. T. L. acknowledge support from the WisCAMP program, funded by National Science Foundation (US) Grants #11911284 and #1400815.

References

- 1 J. Rose, Molecular complexes, 1st edn, Pergamon Press, Oxford, 1967.
- 2 R. S. Mulliken and W. B. Person, Molecular complexes: A lecture and reprint volume, Wiley-Interscience, New York, 1969.
- 3 Y. Zhao and D. G. Truhlar, The M06 suite of density functionals for main group thermochemistry, thermochemical kinetics, noncovalent interactions, excited states, and transition elements: Two new functionals and systematic testing of four M06-class functionals and 12 other functionals, Theor. Chem. Acc., 2008, 120(1-3), 215-241.
- 4 Y. Zhao and D. G. Truhlar, Density functionals with broad applicability in chemistry, Acc. Chem. Res., 2008, 41(2), 157–167.
- 5 V. Jonas, G. Frenking and M. T. Reetz, Comparative theoretical study of the Lewis acid-base complexes of BH₃, BF₃, BCl₃, AlCl₃, and SO₂, J. Am. Chem. Soc., 1994, 116(19), 8741-8753.
- 6 G. Frenking, K. Wichmann, N. Fröhlich, C. Loschen, M. Lein and J. Frunzke, et al., Towards a rigorously defined quantum chemical analysis of the chemical bond in donoracceptor complexes, Coord. Chem. Rev., 2003, 238, 55-82.
- 7 J. S. Murray, P. Lane, T. Clark, K. E. Riley and P. Politzer, Sigma-holes, pi-holes and electrostatically-driven interactions, J. Mol. Model., 2012, 18(2), 541-548.

8 T. Clark, Sigma-holes, Wiley Interdiscip. Rev.: Comput. Mol. Sci., 2013, 3(1), 13-20.

- 9 K. J. Donald and M. Tawfik, The weak helps the strong: Sigma-holes and the stability of MF4 center dot base complexes, J. Phys. Chem. A, 2013, 117(51), 14176-14183.
- 10 S. J. Grabowski, π-Hole bonds: boron and aluminum Lewis acid centers, ChemPhysChem, 2015, 16(7), 1470-1479.
- 11 J. A. Phillips, Structural and energetic properties of nitrile-BX3 complexes: Substituent effects and their impact on condensedphase sensitivity, Theor. Chem. Acc., 2016, 136(1), 12.
- 12 K. R. Leopold, M. Canagaratna and J. A. Phillips, Partially bonded molecules from the solid state to the stratosphere, Acc. Chem. Res., 1997, 30(2), 57-64.
- 13 M. A. Dvorak, R. S. Ford, R. D. Suenram, F. J. Lovas and K. R. Leopold, van der Waals vs. covalent bonding: Microwave characterization of a structurally intermediate case, J. Am. Chem. Soc., 1992, 114(1), 108-115.
- 14 B. Swanson, D. F. Shriver and J. A. Ibers, Nature of the donoracceptor bond in acetonitrile-boron trihalides. The structures of the boron trifluoride and boron trichloride complexes of acetonitrile, Inorg. Chem., 1969, 8(10), 2182-2189.
- 15 W. A. Burns and K. R. Leopold, Unusually large gas-solid structure differences - a crystallographic study of HCN-BF3, J. Am. Chem. Soc., 1993, 115(24), 11622-11623.
- 16 J. A. Phillips, J. A. Halfen, J. P. Wrass, C. C. Knutson and C. J. Cramer, Large gas-solid structural differences in complexes of haloacetonitriles with boron trifluoride, Inorg. Chem., 2006, 45(2), 722-731.
- 17 D. J. Giesen and J. A. Phillips, Structure, bonding, and vibrational frequencies of CH₃CN-BF₃: New insight into medium effects and the discrepancy between the experimental and theoretical geometries, J. Phys. Chem. A, 2003, **107**(20), 4009–4018.
- 18 A. R. Buchberger, S. J. Danforth, K. M. Bloomgren, J. A. Rohde, E. L. Smith and C. C. A. Gardener, et al., Condensed-phase effects on the structural properties of FCH2CN-BF3 and ClCH₂CN-BF₃: A matrix-isolation and computational study, J. Phys. Chem. B, 2013, 117(39), 11687-11696.
- 19 H. M. Helminiak, R. R. Knauf, S. J. Danforth and J. A. Phillips, Structural and energetic properties of acetonitrile-group IV (A & B) halide complexes, J. Phys. Chem. A, 2014, 118(24), 4266-4277.
- 20 J. P. Wrass, D. Sadowsky, K. M. Bloomgren, C. J. Cramer and J. A. Phillips, Quantum chemical and matrix-IR characterization of CH3CN-BCl3: A complex with two distinct minima along the B-N bond potential, Phys. Chem. Chem. Phys., 2014, 16(31), 16480-16491.
- 21 J. A. Phillips, S. J. Danforth, N. J. Hora, J. R. Lanska and A. W. Waller, Structural and energetic properties of haloacetonitrile-BCl3 complexes: Computations and matrix-IR spectroscopy, J. Phys. Chem. A, 2017, 121(48), 9252-9261.
- 22 J. Chatt, L. Manojlov and K. W. Muir, X-ray determination of molecular structures of molybdenum(IV) oxi-complexes -Possibility of a new type of isomerism, J. Chem. Soc. D: Chem. Commun., 1971, 13, 655.

23 G. Parkin, Do bond-stretch isomers really exist?, Acc. Chem. Res., 1992, 25(10), 455-460.

- 24 S. Pan, G. Jana, R. Saha, L. L. Zhao and P. K. Chattaraj, Intriguing structural, bonding and reactivity features in some beryllium containing complexes, Phys. Chem. Chem. Phys., 2020, 22, 47.
- 25 M. Homray, S. Mondal, A. Misra and P. K. Chattaraj, Bond stretch isomerism in Be-3(2-) driven by the Renner-Teller effect, Phys. Chem. Chem. Phys., 2019, 21(15), 7996-8003.
- 26 S. J. Grabowski, The nature of triel bonds, a case of B and Al centres bonded with electron rich sites, Molecules, 2020, 25, 4668.
- 27 G. Feng, Q. Gou, L. Evangelisti, J. U. Grabow and W. Caminati, Pulsed jet Fourier transform microwave spectroscopy of the BF3-CO complex, J. Mol. Spectrosc., 2017, 335, 80-83.
- 28 M. J. Frisch GWT, H. B. Schlegel, G. E. Scuseria, M. A. Robb JRC, G. Scalmani, V. Barone, B. Mennucci, G. A. Petersson HN, M. Caricato, X. Li, H. P. Hratchian, A. F. Izmaylov JB, G. Zheng, J. L. Sonnenberg, M. Hada, M. Ehara KT, R. Fukuda, J. Hasegawa, M. Ishida, T. Nakajima, Y. Honda OK, H. Nakai, T. Vreven, J. A. Montgomery, Jr., et al., Gaussian 09, Revision B.01, Gaussian, Inc., Wallingford CT, 2010.
- 29 M. J. Frisch GWT, H. B. Schlegel, G. E. Scuseria, M. A. Robb JRC, G. Scalmani, V. Barone, G. A. Petersson HN, X. Li, M. Caricato, A. V. Marenich, J. Bloino BGJ, R. Gomperts, B. Mennucci, H. P. Hratchian, J. V. Ortiz AFI, J. L. Sonnenberg, D. Williams-Young, F. Ding FL, F. Egidi, J. Goings, B. Peng, A. Petrone, et al. Gaussian 16, Revision C.01, Gaussian, Inc., Wallingford CT, 2019.
- 30 Y. Zhao, N. E. Schultz and D. G. Truhlar, Design of density functionals by combining the method of constraint satisfaction with parametrization for thermochemistry, thermochemical kinetics, and noncovalent interactions, J. Chem. Theory Comput., 2006, 2(2), 364-382.
- 31 J. D. Chai and M. Head-Gordon, Long-range corrected hybrid density functionals with damped atom-atom dispersion corrections, Phys. Chem. Chem. Phys., 2008, 10(44), 6615-6620.
- 32 Y. Zhao and D. G. Truhlar, Exploring the limit of accuracy of the global hybrid meta density functional for main-group thermochemistry, kinetics, and noncovalent interactions, J. Chem. Theory Comput., 2008, 4(11), 1849-1868.
- 33 R. Peverati and D. G. Truhlar, Improving the accuracy of hybrid meta-GGA density functionals by range separation, J. Phys. Chem. Lett., 2011, 2(21), 2810-2817.

- 34 R. Peverati and D. G. Truhlar, Screened-exchange density functionals with broad accuracy for chemistry and solid-state physics, Phys. Chem. Chem. Phys., 2012, 14(47), 16187-16191.
- 35 C. J. Cramer, Essentials of computational chemistry: theories and models, Wiley.com, 2005.
- 36 G. Herzberg, Molecular spectra and molecular structure, 2nd edn, R.E. Krieger Pub. Co., Malabar, FL, 1989.
- 37 A. W. Waller, N. M. Weiss, D. A. Decato and J. A. Phillips, Structural and energetic properties of haloacetonitrile -GeF₄ complexes, *J. Mol. Struct.*, 2017, **1130**, 984–993.
- 38 N. P. Wells and J. A. Phillips, Infrared spectrum of CH₃CN-BF₃ in solid argon, J. Phys. Chem. A, 2002, **106**(8), 1518–1523.
- 39 A. A. Eigner, J. A. Rohde, C. C. Knutson and J. A. Phillips, IR spectrum of CH3CN-BF3 in solid neon: Matrix effects on the structure of a Lewis acid-base complex, J. Phys. Chem. B, 2007, 111(6), 1402-1407.
- 40 M. Mantina, A. C. Chamberlin, R. Valero, C. J. Cramer and D. G. Truhlar, Consistent van der Waals Radii for the Whole Main Group, J. Phys. Chem. A, 2009, 113(19), 5806-5812.
- 41 B. Cordero, V. Gomez, A. E. Platero-Prats, M. Reves, J. Echeverria and E. Cremades, et al., Covalent radii revisited, Dalton Trans., 2008, 2832-2838.
- 42 J. A. Phillips and C. J. Cramer, Quantum chemical characterization of the structural and energetic properties of HCN-BF3, J. Chem. Theory Comput., 2005, 1(5), 827-833.
- 43 E. L. Smith, D. Sadowsky, J. A. Phillips, C. J. Cramer and D. J. Giesen, A short yet very weak dative bond: Structure, bonding, and energetic properties of N2-BH3, J. Phys. Chem. A, 2010, 114(7), 2628-2636.
- 44 T. Brinck, J. S. Murray and P. Politzer, Computational analysis of the bonding in boron-trifulride and borontrichloride and their complexes with ammonia, Inorg. Chem., 1993, 32(12), 2622-2625.
- 45 E. L. Smith, D. Sadowsky, C. J. Cramer and J. A. Phillips, Structure, bonding, and energetic properties of nitrile-borane complexes: RCN-BH₃, J. Phys. Chem. A, 2011, 115(10), 1955-1963.
- 46 J. Gebicki and J. Liang, IR evidence for the formation of weakly bound complexes BF₃-CO and BF₃-N₂, J. Mol. Struct., 1984, 117(3-4), 283-286.
- 47 L. M. Nxumalo and T. A. Ford, The boron trifluoride-carbon monoxide complex: A matrix-isolation infrared spectroscopic and ab initio molecular-orbital theoretical study, South Afr. J. Chem., 1995, 48(1-2), 30-38.